TURBULENT DRAG REDUCTION DUE TO LAMINAR WALL-JET FLOWS, SIMULATING EFFLUX FROM FISH GILLS

Tadashi Nakano
Department of Mechanical and System Engineering
Kyoto Institute of Technology
Matsugasaki, Sakyo-ku, Kyoto 606-8585, Japan

Yoshimichi Hagiwara
Department of Mechanical and System Engineering
Kyoto Institute of Technology
Matsugasaki, Sakyo-ku, Kyoto 606-8585, Japan
yoshi@kit.ac.jp

ABSTRACT

We have carried out direct numerical simulation for turbulent flow with the injection of laminar wall jets in order to simulate efflux flow from the gills of swimming fish. The bulk-mean velocity of the jet is lower than the maximum velocity of main flow. It is found that a decrease in the turbulence intensity and the negative velocity gradient due to the jet flow lead to a decrease in the Reynolds shear stress, which causes a decrease in the turbulence intensities. A 3.3% reduction of spatiotemporal averaged value of wall shear stress is obtained in the case where the main-flow Reynolds number based on the friction velocity is 150 and the bulk-mean velocity of the jet is five times the friction velocity. This is due to fact that the jet flow weakens the sweep events in a wide region downstream from the place where the jet is located.

INTRODUCTION

The reduction of drag acting on a moving body in fluid has been a focus of research for many years, with the aim of saving energy and enabling faster movement. In the cases of aircrafts and ship, the pressure drag acting on these bodies has already been reduced, while the reduction of friction drag is still widely studied. This is because the friction drag is predominant in the total drag acting on the bodies. Gad-el-Hak (2000) classified techniques proposed for the friction-drag reduction into the following three categories: (1) reduction of near-wall momentum, (2) introduction of foreign substances, and (3) methods involving geometry. Jet injection, polymers and riblets respectively are typical examples of these categories.

Some of the studies and techniques concerning the friction-drag reduction were inspired by fish and sea mammals. Some three-dimensional riblets were based on shark skins (e.g. Bechert et al. 2000). Similarly some compliant surfaces were inspired by dolphins' skin (e.g. Gad-el-Hak et al. 1984, Matsumura et al. 2007). Nevertheless, as far as the present authors know, little discussion has occurred about the drag acting on big fish, such as tuna and bonito, so far. The shear stress on the body surface of some species of tuna is much higher than that on the body surface of sharks and dolphins because the species of tuna can swim faster than any other fish and sea mammals.

To exchange gas in the micro vessels of gills, seawater is continuously sucked in from a fast-swimming fish's mouth and is discharged from a space between the lids of the gills and the fish's body. Efflux flow of seawater is formed at the outlet of the gills. This efflux flow interacts with seawater along the body surface of the fish. As far as the present authors know, this interaction has not yet been studied widely. Thus, it has not yet been clarified whether or not the turbulent friction drag increases or decreases due to the efflux.

The present authors have thought that the efflux flow is simulated with wall jets. As is reviewed in the book written by Gad-el-Hak (2000), many studies on the wall jet have already been carried out to control air flow turbulence and air flow separation. Most of the studies show increases in the momentum in the streamwise direction and thus the friction drag. This is because the maximum jet velocity is high in order to attenuate the flow separation. On the other hand, Howard et al. (1975) predicted a decrease in the friction coefficient in the case of multiple wall jets for an ogive-cylinder body. The effects of wall jets and thus the efflux flow on turbulent friction drag cannot be understood from all the results previously obtained. Thus, in the present study, we carry out direct numerical simulation on turbulent flow with laminar wall jets to elucidate the effects of the efflux on turbulence structure and wall shear stress.

COMPUTATIONAL METHOD

Assumptions

We dealt with water in a small rectangular region on the body surface of a swimming fish. An observer moving with the fish sees that water flows into the region from a side surface and flows out from the opposite side surface. The water flow was assumed to be turbulent. The body surface was assumed to be flat and the lid of the gills was assumed to be flat and two-dimensional in the small region. The thickness of the gills' lid was assumed to be negligible. It was also assumed that the lid is at a slight angle to the surface. The efflux flow was simulated with a laminar steady jet which issued from a two-dimensional opening between the edge of the lid and body surface. The axis of the wall jet was in parallel with the surface.

Computational Domains

We carried out the following two computations: the main computation and the auxiliary computation. Figure 1 shows the domains for the two computations. The domain for the auxiliary computation, shown in Fig. 1(a), is a rectangular box of $4\pi h \times h \times \pi h$. The x-, y- and z-axes were positioned in the streamwise, upward and transverse directions respectively. The bottom wall of the domain corresponds to a part of the fish body surface. A projection, which has a uniform triangular cross section in the transverse direction, exists on the bottom wall. The height of the projection, $\delta = 0.02h$, corresponds to the height of the space between the lid of the gills and the fish's body. The ascending surface of the projection corresponds to the lid surface.

The domain for the main computation, shown in Fig. 1(b), is a rectangular box of $2\pi h \times h \times \pi h$. The x-, y- and z-axes were positioned in the streamwise, upward and transverse directions respectively. The bottom wall of the domain corresponds to the fish body surface downstream of the gills. At the upstream boundary of the domain, a laminar jet with a parabolic velocity profile is issued from the narrow area of $0 < y < \delta$ at any time. A turbulent velocity field is given for the remaining area of the upstream boundary.

Schemes and Grid Arrangement

The Navier-Stokes equations were discretized with staggered grid systems. The grid spacing was identical in the z-direction. The spacing was identical in the x-direction in the auxiliary computation, while the spacing increased from the upstream boundary in the x-direction in the main computation. Also the spacing increased from the upper and lower boundaries in the y-direction in the two computations. The second-order central difference scheme based on an interpolation method (Kawamura 1995) was used to obtain discrete forms of nonlinear terms, while the same scheme without the interpolation method was used to obtain discrete forms of viscous terms. In order to evaluate the time evolution of these terms, the third-order Runge-Kutta method was adopted. The pressure Poisson equation was solved with the successive over-relaxation method together with a multi-grid method (Arakawa 1994) in the main computation, while it was solved with the fast Fourier transform (FFT) in the auxiliary computation. In order to evaluate the time evolution of the pressure-gradient term, a fractional time-step method was employed.

Boundary Conditions

A non-slip boundary condition was adopted for the lower walls of the main and auxiliary computations. A free-slip boundary condition was adopted for the upper walls, which are imaginary boundaries in seawater. The periodic boundary condition was applied for the walls perpendicular to the z-axis.

In the main computation, at the downstream boundary, a convection outflow condition was applied. On the other hand, at the upstream boundary, the velocity of the main flow was assigned at any time step at the upstream boundary except for the area of the wall jet. For this purpose, a database was generated by means of the auxiliary computation. The database consists of four million sets of velocity vectors on the cross section above the crest of the projection. In the auxiliary computation, the periodic boundary condition was applied in the streamwise direction. An immersed boundary method developed by Kim et al. (2001) was adopted to calculate the boundary values at the projection surfaces.

Computational Conditions

The Reynolds number was $Re = hu_{\tau 0}/\nu = 200$ and 150, where ν is the kinematic viscosity and $u_{\tau 0}$ is the friction velocity without jets. Statistical quantities were obtained for the periods of $4000\nu/u_{\tau 0}^2$. We carried out computations for five different cases, changing the jets' velocities and flow Reynolds number as shown in Table 1. Note that the bulk mean velocity of the jet is much lower than the maximum velocity of the main flow.

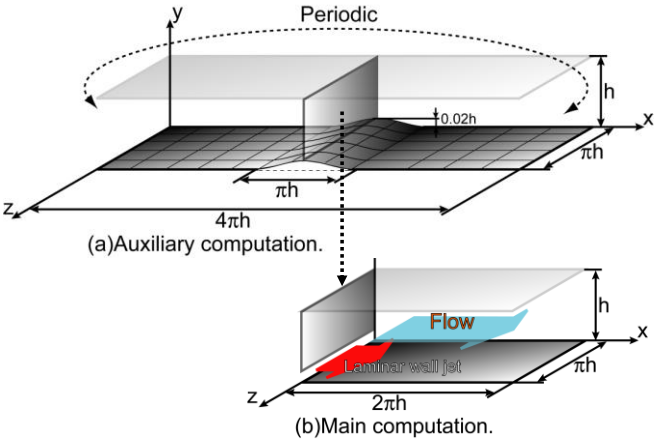

Figure 1. Computational domains: (a) auxiliary computation, (b) main computation.

Table 1. Computational conditions.

case	*Re*	bulk-mean jet velocity
0	150	0
1	150	$5u_{\tau 0}$
2	150	$10u_{\tau 0}$
3	200	0
4	200	$10u_{\tau 0}$

RESULTS AND DISCUSSION

Mean Velocities

Figure 2 shows the profiles of mean velocity at ten different locations in the streamwise direction. It is found from Fig. 2(a) and (b) that the mean velocities both in the x- and y-directions in the cases with jets differ noticeably from those in the cases without jets, particularly in a region downstream from the upstream boundary ($0 < x < 2\pi h/5$, i.e. $0 < x^+ < 188$) in the case of $Re = 150$. The effects of the wall jet on the mean velocities are also observed in a region downstream from the upstream boundary ($0 < x < 2\pi h/5$, i.e. $0 < x^+ < 251$) in the case of $Re = 200$ (See Fig. 2(c) and 2(d)).

Turbulence Intensities

Figure 3 indicates the profiles of turbulence intensities in the three directions at the same ten locations as those of the mean velocities mentioned above. In Figs. 3(a), 3(b) and 3(c), the turbulence intensities in the cases with jets are found to be lower than those in the cases without jets in a region of $0 < x < 3\pi h/5$ ($0 < x^+ < 283$) and $0 < y < 0.15h$ ($0 < y^+ < 22.5$) in the case of $Re = 150$. A similar effect of the wall jet on the turbulence intensities is also observed in a region of $0 < x < 3\pi h/4$ ($0 < x^+ < 471$) and $0 < y < 0.15h$ ($0 < y^+ < 30$) in the case of $Re = 200$. (The intensities are not shown except for the streamwise intensity displayed in Fig. 3(d).)

Reynolds Shear Stresses

Figure 4 depicts the profiles of the Reynolds shear stress $-\overline{u'v'}$ at the ten locations in the streamwise direction. The computational results obtained by Yamamoto et al. (2001) for an open-channel flow are also shown in Fig. 4(b). The Reynolds shear stress in the cases with jets are lower than those in the cases without jets in a region of $0 < x < 3\pi h/5$ ($0 < x^+ < 283$) and $0 < y < 0.2h$ ($0 < y^+ < 30$) in the case of $Re = 150$. A similar effect of the wall jet on the Reynolds shear stress is also seen in a region of $0 < x < 3\pi h/5$ ($0 < x^+ < 377$) and $0 < y < 0.2h$ ($0 < y^+ < 40$) in the case of $Re = 200$.

The term of $-\overline{v'^2}\left(\partial\bar{u}/\partial y\right)$ is predominant among the production terms in the governing equation of the Reynolds shear stress. The mean velocity gradient is negative near the upper part of the wall jet due to the parabolic velocity distribution. Thus the production of the Reynolds shear stress is attenuated by the upper part of the wall jet. This attenuation and a decrease in the turbulence intensity in the wall-normal direction cause a decrease in the Reynolds shear stress. Similarly, the term of $-\overline{u'v'}\left(\partial\bar{u}/\partial y\right)$ is predominant among the production terms in the governing equation of the turbulent kinetic energy k. The production of k is attenuated by the negative velocity gradient at the upper part of the wall jet and a decrease in the Reynolds shear stress. This attenuation causes a decrease in the turbulence intensities.

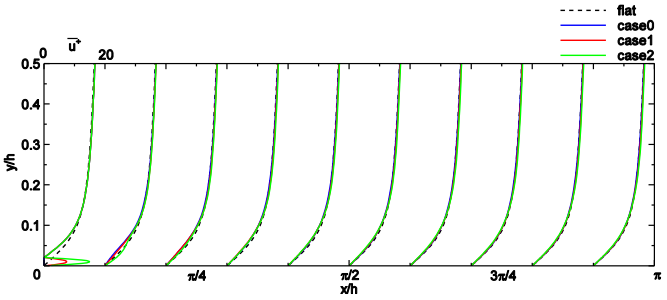

(a) streamwise mean velocity in the case of Re=150.

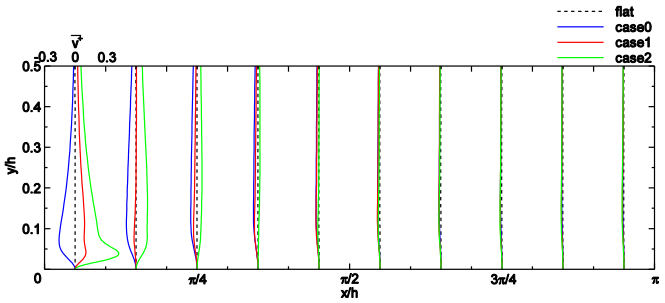

(b) wall-normal mean velocity in the case of Re=150.

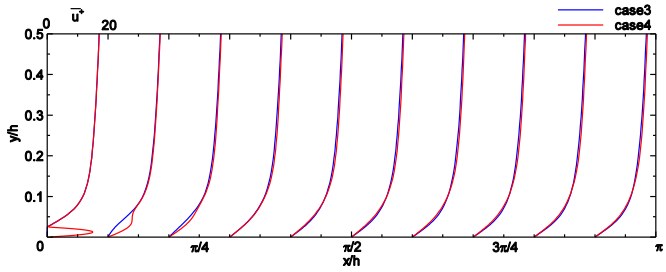

(c) streamwise mean velocity in the case of Re=200.

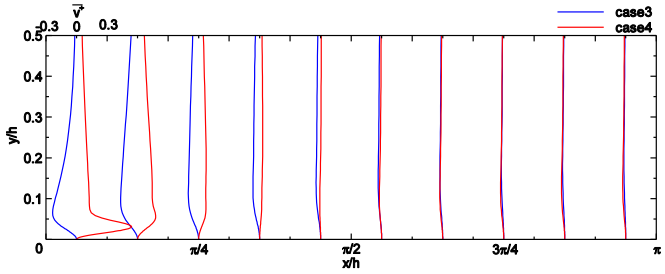

(d) wall-normal mean velocity in the case of Re=200.

Figure 2. Profiles of mean velocity.

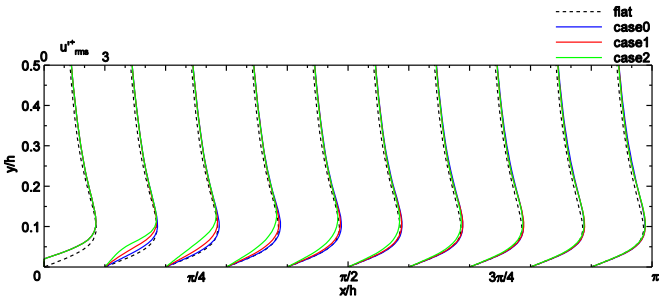

(a) streamwise turbulence intensity in the case of *Re*=150.

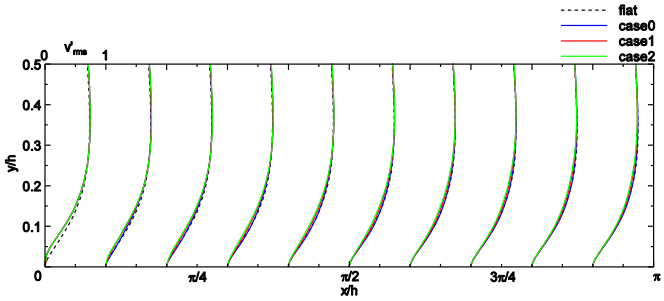

(b) wall-normal turbulence intensity in the case of *Re*=150.

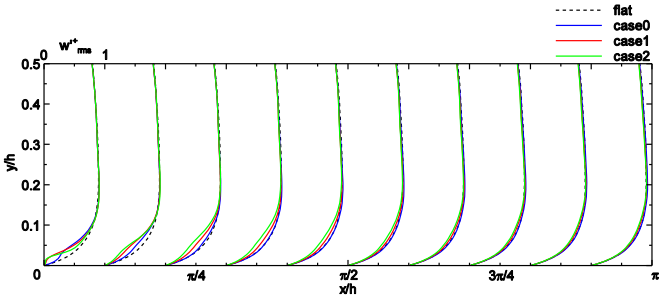

(c) transverse turbulence intensity in the case of *Re*=150.

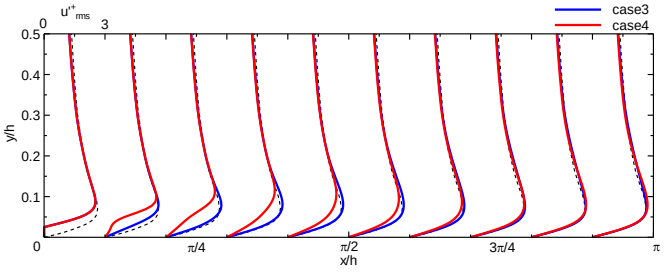

(d) streamwise turbulence intensity in the case of *Re*=200.

Figure 3. Profiles of turbulence intensities.

Local Wall Shear Stress

Figure 5 shows the streamwise changes in local wall shear stresses. The wall shear stress is normalized with that in the case without jets. In the case of *Re* = 150, as shown in Fig. 5(a), the wall shear stress is high near the upstream boundary. This is due to the high velocity gradient in the jets. However, the wall shear stress decreases noticeably within short distances from the jets. It is lower than that in the case of the flat wall at x = $\pi h/16$, i.e. x^+ = 29 in case 1. Also, it is lower than that in the case of the flat wall at x = $3\pi h/16$, i.e. x^+ = 88 in case 2. This suggests that the viscous shear stress and the Reynolds shear stress are affected slightly by the jet flow even in a region far downstream. A similar effect of the wall jet on the wall shear stress is seen in the case of *Re* = 200: the wall shear stress is lower than that in the case of the flat wall at x = $3\pi h/16$, i.e. x^+ = 117 in case 4, as shown in Fig. 5(b).

Integral-mean Values of Wall Shear Stress

The integral-mean values of wall shear stress over a certain area in cases 2 and 4 are higher than that in the case of the flat wall. On the other hand, the integral mean value in case 1 is lower than that in the case of the flat wall, if the surface for the integration is wider than $0.4\pi h \times \pi h$. The integral mean value decreases to 0.967 when the surface is equal to the whole lower wall. This clearly shows that the injection of a weak laminar wall jet is effective for the reduction of friction drag in the region downstream from the place where the jet is located.

The local shear stress far from the location of the jet decreases in the case of higher flow rate of the jet compared with that in the case of lower flow rate of the jet as shown in Fig. 5(a). However, the increase in the bulk mean velocity of the laminar wall jet does not contribute to the decrease in the integral-mean value of wall shear stress. This is because the increase in the local wall shear stress is noticeable near the location of the jet in the case of higher flow rate of the jet (See Fig. 5(a)).

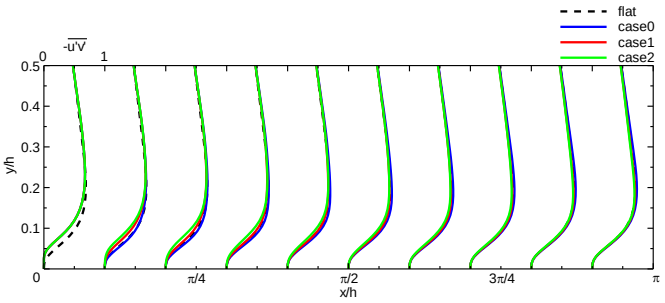

(a) in the case of *Re*=150.

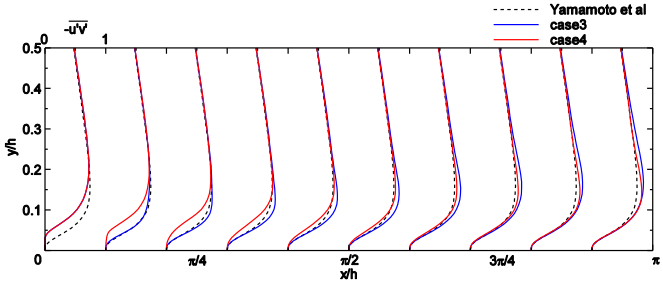

(b) in the case of *Re*=200.

Figure 4. Profiles of Reynolds shear stresses.

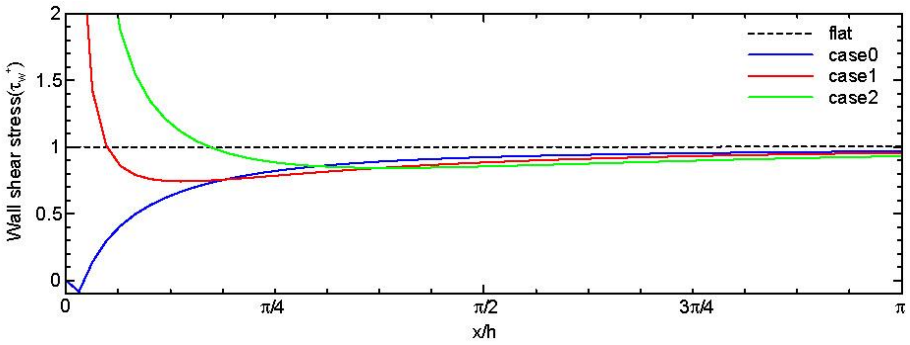

(a) in the case of *Re*=150.

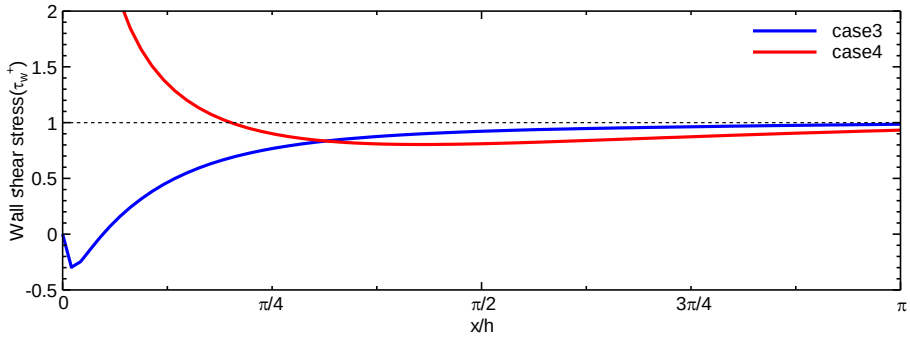

(b) in the case of *Re*=200.

Figure 5. Streamwise changes in local wall shear stress.

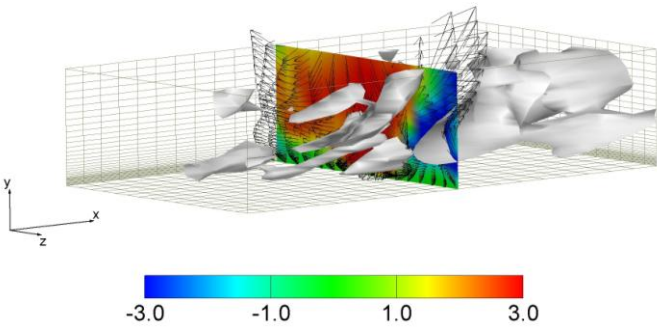

(a) bird's-eye view

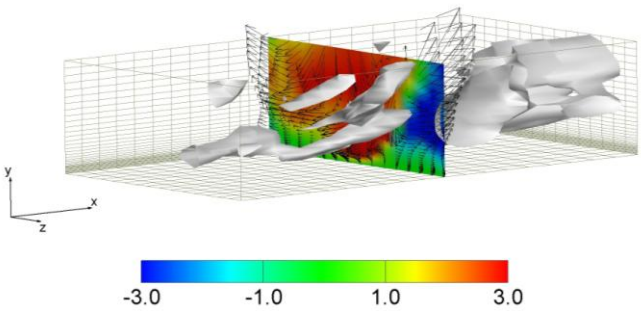

(a) bird's-eye view

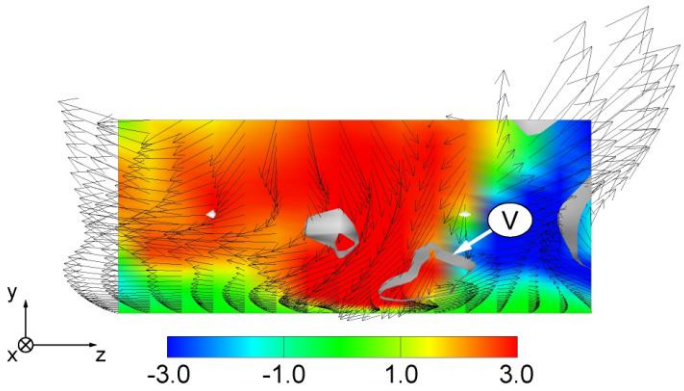

(b) cross-section

Figure 6. Hairpin vortices and fluctuating velocities (case 0).

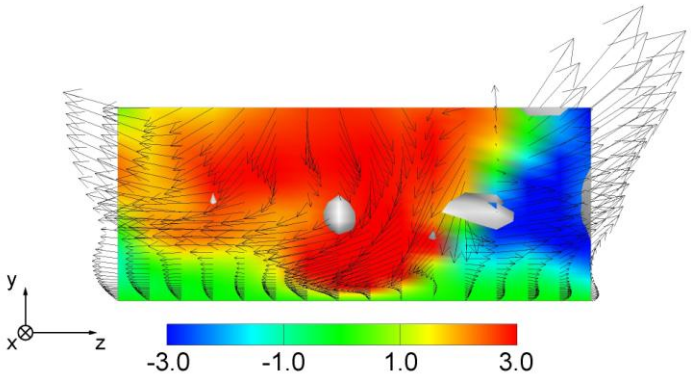

(b) cross-section

Figure 7. Hairpin vortices and fluctuating velocities (case 2).

Modification of Coherent Structure

The discussion of the Reynolds shear stress in Section 3.3 is not sufficient for the explanation of the integral-mean value of the wall shear stress partly because the mean velocity gradient due to the wall jet is positive adjacent to the wall and partly because the Reynolds shear stress recovers at around x = 3π*h*/5. To elucidate the decrease in the integral-mean value of the wall shear stress, we focus on the near-wall coherent structure.

Figure 6 shows the color contours of fluctuating flow and hairpin vortices near the surface in case 0. The identification of vortices is the same as that developed by Jeong and Hussain (1995). The red area indicates the higher values of the fluctuating velocity, which express the cross-sectional view of high-speed streaks. The blue area indicates the lower values of the fluctuating velocity, which express the cross-sectional view of low-speed streaks. The grey areas show the hairpin vortices. Figure 6(a) indicates a bird's-eye view, while Fig. 6(b) indicates the cross-section at x = π*h*/4, i.e. $x^+ = 118$ at $t^+ = 101$. The arrows show the fluctuating velocities. Upward strong flow is seen in the blue region. This is a typical event of "ejection". This ejection was generated by the hairpin vortex with a "V" symbol and an adjacent hairpin vortex. On the other hand, downward flow is seen in the red region. This is a typical event of "sweep". This sweep was generated by the hairpin vortex with the "V" symbol and the other adjacent hairpin vortex.

Figure 7 depicts the color contours of fluctuating flow and hairpin vortices near the surface in case 2. The identification of vortices, the definition of colors, the location of the cross section and the instant are the same as those mentioned above. Upward strong flow is seen in the blue region. However, the cross-sectional area of the hairpin vortex with the "V" symbol is smaller than that in case 0. Furthermore, downward flow seen in the red region is weak compared with that seen in Fig. 6(b). The red region is slightly farther from the wall compared with that in Fig. 6(b). These show clearly that the sweep is weaker than that in case 0. Thus, the jet flow weakens the sweep events. The decrease in the Reynolds shear stress in the upper part of the buffer region mentioned in Section 3.3 also contributes to the attenuation of the sweep events. The decrease in the Reynolds shear stress and the attenuation of the sweep events are the reason for the decrease in the wall shear stress due to the jet flow. It is noted that similar results were obtained in the case of *Re* = 200.

CONCLUSIONS

We have carried out direct numerical simulation for turbulent flow with the injection of laminar wall jets. The main conclusions obtained are as follows:

(1) The regions are limited where the profiles of the mean velocities, turbulence intensities and the Reynolds shear stress are modified by the laminar wall jet.

(2) A decrease in the turbulence intensity $\overline{v'^2}$ and the negative velocity gradient due to the jet flow leads to a decrease in the Reynolds shear stress $-\overline{u'v'}$. This decrease leads to a decrease in the turbulent kinetic energy and thus $\overline{v'^2}$. This cyclic mechanism is the reason for the modification of turbulence quantities.

(3) A 3.3% reduction of integral-mean value of the wall shear stress is obtained in the case where *Re* = 150 and the bulk-mean velocity of the jet flow is five times the friction velocity.

(4) The reduction of the spatiotemporal value of the wall shear stress is caused by the jet flow which weakens the sweep events in a wide region downstream from the place where the jet is located.

ACKNOWLEDGMENTS

The authors thank Mr. Mimori, an aquarist of the Tokyo Sea Life Park, to his comments and images of tuna.

REFERENCES

Arakawa, C., 1994, *Computational Fluid Dynamics for Engineering* (in Japanese), pp. 171-185, University of Tokyo Press.

Bechert, D. W., Bruse, M. and Hage, W., 2000, "Experiments with three-dimensional riblets as an idealized model of shark skin", *Experiments in Fluids*, Vol. 28, pp. 403-412.

Gad-el-Hak, M., Blackwelder, R. F. and Riley, J. J., 1984, "On the interaction of compliant coatings with boundary layer flows", *Journal of Fluid Mechanics*, Vol. 140, pp. 257-280.

Gad-el-Hak, M., 2000, *Flow Control: passive, active and reactive flow management*, pp. 150-188, pp. 205-228, Cambridge University Press.

Howard, F. G., Hefner, J. N. and Srokowski, A. J., 1975, "Multiple slot skin friction reduction", *Journal of Aircraft*, Vol. 12, pp. 753-754.

Jeong, J. and Hussain, F., 1995, "On the identification of a vortex", *Journal of Fluid Mechanics*, Vol. 285, pp. 69-94.

Kawamura, H., 1995, "Direct numerical simulation of turbulence by finite difference scheme", in *The Recent Development in Turbulence Research* (ed. by Z. S. Zhang and Y. Miyake), pp. 54-60, International Academic Publishers.

Kim, J., Kim, D. and Choi, H., 2001, "An immersed-boundary finite-volume method for simulations of flow in complex geometries", *Journal of Computational Physics*, Vol. 171, pp. 132-150.

Matsumura, R., Koyama, S. and Hagiwara, Y., 2007, "Turbulent drag reduction by wall deformation synchronized with flow acceleration", *IUTAM Symposium on Computational Physics and New Perspectives in Turbulence* (ed. by Y. Kaneda), pp.385-390.

Yamamoto, Y., Kunugi, T. and Serizawa A., 2001, "Turbulence statistics and scalar transport in an open-channel flow", *Journal of Turbulence*, Vol. 2, article no. 010, pp.1-16.